Spectroscopic Identification of Oxonium and Carbenium Ions of Protonated Phenol in the Gas Phase: IR Spectra of Weakly Bound $C_6H_7O^+$−L Dimers (L = Ne, Ar, N_2)

Nicola Solcà and Otto Dopfer*

Contribution from the Institute for Physical Chemistry, University of Würzburg, Am Hubland, D-97074 Würzburg, Germany

Received October 11, 2003; E-mail: dopfer@phys-chemie.uni-wuerzburg.de

Abstract: Structural isomers of isolated protonated phenol ($C_6H_7O^+$) are characterized by infrared (IR) photodissociation spectroscopy of their weakly bound complexes with neutral ligands L (L = Ne, Ar, N_2). IR spectra of $C_6H_7O^+$−L recorded in the vicinity of the O−H and C−H stretch fundamentals carry unambiguous signatures of at least two $C_6H_7O^+$ isomers: the identified protonation sites of phenol include the O atom (oxonium ion, O-$C_6H_7O^+$) and the C atoms of the aromatic ring in the *ortho* and/or *para* position (carbenium ions, o/p-$C_6H_7O^+$). In contrast, protonation at the *meta* and *ipso* positions is not observed. The most stable $C_6H_7O^+$−L dimer structures feature intermolecular H-bonds between L and the OH groups of O-$C_6H_7O^+$ and o/p-$C_6H_7O^+$. Extrapolation to zero solvation interaction yields reliable experimental vibrational frequencies of bare O-$C_6H_7O^+$ and o/p-$C_6H_7O^+$. The interpretation of the $C_6H_7O^+$−L spectra, as well as the extrapolated monomer frequencies, is supported by B3LYP and MP2 calculations using the 6-311G-(2df,2pd) basis. The spectroscopic and theoretical results elucidate the effect of protonation on the structural properties of phenol and provide a sensitive probe of the activating and *ortho/para* directing nature of the OH group observed in electrophilic aromatic substitution reactions.

1. Introduction

The characterization of reactive intermediates is of fundamental interest in organic chemistry, because information about structural and energetic properties of such transient species is required to understand and possibly control the dynamics and selectivity of chemical processes.[1−3] Protonated aromatic molecules (AH^+) are pivotal intermediates in electrophilic aromatic substitution (EAS) reactions, one of the most important reaction mechanisms of aromatic molecules. The elucidation of mechanistic details of EAS reactions by characterizing AH^+ is a challenging and active area of research.[4] In addition, protonation and deprotonation of aromatic molecules are important biochemical processes.[5] In the condensed phase, AH^+ has mainly been investigated by NMR, IR, and UV−vis spectroscopy, as well as X-ray crystallography.[6−10] Although these studies have characterized solvated AH^+, they revealed that many of their

properties strongly depend on the environment (such as solvent molecules or counterions).[11] For example, the preference for protonation of phenol (C_6H_6O) at the aromatic ring or at the OH group studied by low-temperature NMR spectroscopy shows a drastic solvent and temperature dependence.[12]

Gas-phase studies are required to separate intrinsic molecular properties from interfering solvation effects.[13−17] To date, nearly all investigations of isolated AH^+ are based on mass spectrometric or theoretical techniques. Structural characterization via mass spectrometry is, however, indirect, often disputable, and only in a few cases unambiguous.[14,15] On the other hand, spectroscopic techniques (and in particular IR spectroscopy) can be sensitive tools to unambiguously determine protonation site(s) in AH^+. Early unstructured electronic spectra of AH^+ trapped in an ICR cell did not provide any isomer-specific information of isolated AH^+.[18,19] Recently, structured IR spectra of AH^+ (cluster) ions were recorded for the first time to yield unambiguous information about the protonation sites of AH^+ in the gas phase observed under controlled solvation conditions. The systems investigated so far include protonated benzene

(1) March, J. *Advanced Organic Chemistry: Reactions, Mechanisms, and Structure*; Wiley: New York, 1992.
(2) Carey, F. A.; Sundberg, R. J. *Advanced Organic Chemistry*; Plenum Press: New York, 1993.
(3) Ohtaki, H.; Radnai, T. *Chem. Rev.* **1993**, *93*, 1157.
(4) Lenoir, D. *Angew. Chem., Int. Ed.* **2003**, *42*, 854.
(5) Jeffrey, G. A.; Saenger, W. *Hydrogen Bonding in Biological Systems*; Springer: Heidelberg, 1991.
(6) Perkampus, H. H.; Baumgarten, E. *Angew. Chem., Int. Ed. Engl.* **1964**, *3*, 776.
(7) Brouwer, D. M.; Mackor, E. L.; MacLean, C. Arenonium Ions. In *Carbonium Ions*; Olah, G. A., Schleyer, P. v. R., Eds.; Wiley: New York, 1970; Vol. II.
(8) Dewey, T. X.; Barich, H.; Torres, P. D.; Haw, J. F. *J. Am. Chem. Soc.* **1997**, *119*, 406.
(9) Hubig, S. M.; Kochi, J. K. *J. Org. Chem.* **2000**, *65*, 6807.
(10) Reed, C. A.; Kim, K. C.; Stoyanov, E. S.; Stasko, D.; Tham, F. S.; Mueller, L. J.; Boyd, P. D. W. *J. Am. Chem. Soc.* **2003**, *125*, 1796.

(11) Esteves, P. M.; de M. Carneiro, J. W.; Cardoso, S. P.; Barbosa, A. G. H.; Laali, K. K.; Rasul, G.; Prakash, G. K. S.; Olah, G. A. *J. Am. Chem. Soc.* **2003**, *125*, 4836.
(12) Olah, G. A.; Mo, Y. K. *J. Org. Chem.* **1973**, *38*, 3.
(13) Weinkauf, R.; Schermann, J. P.; de Vries, M. S.; Kleinermanns, K. *Eur. Phys. J. D* **2002**, *20*, 309.
(14) Speranza, M. *Mass Spectrom. Rev.* **1992**, 73.
(15) Kuck, D. *Mass Spectrom. Rev.* **1990**, 583.
(16) Fornarini, S. *Mass Spectrom. Rev.* **1997**, 365.
(17) Fornarini, S.; Crestoni, M. E. *Acc. Chem. Res.* **1998**, *31*, 827.
(18) Freiser, B. S.; Beauchamp, J. L. *J. Am. Chem. Soc.* **1976**, *98*, 3136.
(19) Freiser, B. S.; Beauchamp, J. L. *J. Am. Chem. Soc.* **1977**, *99*, 3214.

(C$_6$H$_7$$^+$),[20−22] protonated phenol (C$_6$H$_7$O$^+$),[23] and protonated fluorobenzene (C$_6$H$_6$F$^+$).[24,25] All of these investigations are based on sensitive IR photodissociation (IRPD) techniques, which overcome the problems of producing sufficient ion concentrations required for spectroscopic experiments.[26]
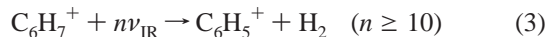
IRPD spectroscopy exploits the fragmentation of a (cluster) ion after resonant absorption of one or more IR photons. For AH$^+$ ions with a low appearance potential for the lowest dissociation channel, IRPD can be achieved under single photon absorption conditions. For example, the fluoronium isomer of C$_6$H$_6$F$^+$ (F-C$_6$H$_6$F$^+$) was selectively detected by IRPD into C$_6$H$_5$$^+$ and HF upon absorption of one IR photon in the 3 μm range:[24]

$$F\text{-C}_6\text{H}_6\text{F}^+ + \nu_{IR} \rightarrow \text{C}_6\text{H}_5^+ + \text{HF} \qquad (1)$$

The more stable carbenium ions of C$_6$H$_6$F$^+$, C-C$_6$H$_6$F$^+$, were not detected in this experiment, because the energy of a single IR photon is insufficient to break any of their strong covalent bonds.[24] Alternatively, spectral features of AH$^+$ can also be inferred by adopting the "messenger" approach,[26,27] in which properties of molecular ions are derived from the characterization of their weakly bound clusters with one or more neutral ligands L, AH$^+$−L$_n$.[20,21,23,25] This approach relies on the fact that either L has only a negligible influence on the properties of AH$^+$ or, if this is not the case, that the intermolecular interaction can be tuned by variation of L (or n) and finally extrapolated to zero (controlled solvation).[26,28−30] The main experimental advantage of the messenger approach is that inert and nonpolar ligands L (such as rare gas atoms or N$_2$) in AH$^+$−L$_n$ can usually be evaporated after resonant absorption of a single IR photon, because the photon energy is sufficient to break the weak intermolecular bonds. For example, the IR spectrum of certain C-C$_6$H$_6$F$^+$ isomers could selectively be derived by IRPD of their weakly bound C-C$_6$H$_6$F$^+$−(N$_2$)$_2$ clusters:[25]

$$C\text{-C}_6\text{H}_6\text{F}^+\text{−(N}_2)_2 + \nu_{IR} \rightarrow \text{C}_6\text{H}_6\text{F}^+ + 2\text{N}_2 \qquad (2)$$

Finally, IRPD of a bare AH$^+$ ion with a high appearance potential for its lowest dissociation channel can also be induced by sequential absorption of several IR photons. For example, the IRPD spectrum of bare C$_6$H$_7$$^+$ was recently obtained by monitoring resonant multiphoton dehydrogenation:[22]

$$\text{C}_6\text{H}_7^+ + n\nu_{IR} \rightarrow \text{C}_6\text{H}_5^+ + \text{H}_2 \quad (n \geq 10) \qquad (3)$$

Such a process requires high IR laser intensities which are provided, for example, by modern free electron lasers.[22]

The present work reports IRPD spectra of protonated phenol (C$_6$H$_7$O$^+$) complexed with a single weakly bound inert ligand L (L = Ne, Ar, N$_2$) in the vicinity of the O−H and C−H stretch
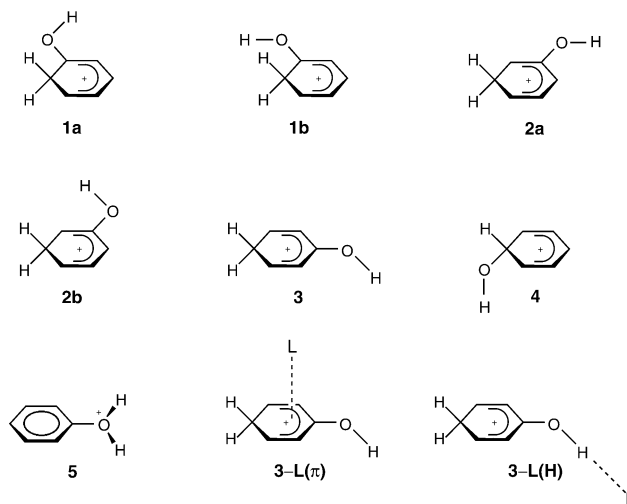

Figure 1. Sketch of possible x-C$_6$H$_7$O$^+$ ions and selected x-C$_6$H$_7$O$^+$−L complexes. Protonation of phenol may occur at the aromatic ring in *ortho* ($x = o$), *meta* ($x = m$), *para* ($x = p$), and *ipso* ($x = i$) positions to form stable carbenium ions (**1**−**4**) or at the oxygen atom (**5**) to form the oxonium ion (**5**). Trans and cis isomers of the OH group with respect to the aliphatic CH$_2$ moiety are possible for o-C$_6$H$_7$O$^+$ and m-C$_6$H$_7$O$^+$ (**1a/b**, **2a/b**). Major binding sites of ligands L to x-C$_6$H$_7$O$^+$ include H-bonding and π-bonding. As an example, H-bound p-C$_6$H$_7$O$^+$−L, **3**−**L(H)**, and π-bound p-C$_6$H$_7$O$^+$−L, **3**−**L(π)**, are shown.

fundamentals. It complements our preliminary IRPD investigation of C$_6$H$_7$O$^+$−Ar$_{1,2}$ in the O−H stretch range.[23] Possible x-C$_6$H$_7$O$^+$ structures are illustrated in Figure 1 (x denotes the site of protonation). Protonation of phenol can occur at the C atoms of the aromatic ring in *ortho*, *meta*, *para*, and *ipso* positions ($x = o$, m, p, and i) to form the carbenium ions **1**−**4** (σ-complexes, Wheland intermediates), and at the O atom ($x = O$) to form the oxonium ion **5**. Moreover, trans and cis isomers of the OH group with respect to the aliphatic CH$_2$ moiety exist for o/m-C$_6$H$_7$O$^+$ (**1a/b** and **2a/b**). Structures **1**−**5** were previously investigated theoretically by quantum chemical methods.[23,31−33] The π-complex, in which the proton binds to the π-electron system of the aromatic ring, is a saddle point on the C$_6$H$_7$O$^+$ potential.[34] Early low-temperature NMR studies identified p-C$_6$H$_7$O$^+$ (**3**) and O-C$_6$H$_7$O$^+$ (**5**) in superacid solutions.[12] Also in the gas phase, carbenium and oxonium ions were invoked to interpret mass spectrometric experiments of C$_6$H$_7$O$^+$, although the protonation site could not directly be determined.[35−39] Proton-transfer equilibrium measurements yield a proton affinity of C$_6$H$_6$O of PA = 816 kJ/mol (assuming **3** as the most stable C$_6$H$_7$O$^+$ structure).[35] The PA for O protonation was estimated as 753 kJ/mol.[36] In contrast to mass spectrometric studies, recent IR spectra of C$_6$H$_7$O$^+$−Ar$_{1,2}$ recorded in the O−H stretch range carry the unambiguous signatures of complexes of **1** and/or **3**, and **5**.[23] In line with theoretical predictions, the IR spectra demonstrate that the most stable C$_6$H$_7$O$^+$−Ar$_{1,2}$ structures have

(20) Solcà, N.; Dopfer, O. *Angew. Chem., Int. Ed.* **2002**, *41*, 3628.
(21) Solcà, N.; Dopfer, O. *Chem.-Eur. J.* **2003**, *9*, 3154.
(22) Jones, W.; Boissel, P.; Chiavarino, B.; Crestoni, M. E.; Fornarini, S.; Lemaire, J.; Maitre, P. *Angew. Chem., Int. Ed.* **2003**, *42*, 2057.
(23) Solcà, N.; Dopfer, O. *Chem. Phys. Lett.* **2001**, *342*, 191.
(24) Solcà, N.; Dopfer, O. *J. Am. Chem. Soc.* **2003**, *125*, 1421.
(25) Solcà, N.; Dopfer, O. *Angew. Chem., Int. Ed.* **2003**, *42*, 1537.
(26) Bieske, E. J.; Dopfer, O. *Chem. Rev.* **2000**, *100*, 3963.
(27) Yeh, L. I.; Okumura, M.; Myers, J. D.; Price, J. M.; Lee, Y. T. *J. Chem. Phys.* **1989**, *91*, 7319.
(28) Nizkorodov, S. A.; Roth, D.; Olkhov, R. V.; Maier, J. P.; Dopfer, O. *Chem. Phys. Lett.* **1997**, *278*, 26−30.
(29) Olkhov, R. V.; Dopfer, O. *Chem. Phys. Lett.* **1999**, *314*, 215.
(30) Solcà, N.; Dopfer, O. *J. Phys. Chem. A* **2001**, *105*, 5637.

(31) Eckert-Maksic, M.; Klessinger, M.; Maksic, Z. B. *Chem. Phys. Lett.* **1995**, *232*, 472.
(32) Tishchenko, O.; Pham-Tran, N. N.; Kryachko, E. S.; Nguyen, M. T. *J. Phys. Chem. A* **2001**, *105*, 8709.
(33) Bouchoux, G.; Defaye, D.; McMahon, T.; Likholyot, A.; Mo, O.; Yanez, M. *Chem.-Eur. J.* **2002**, *8*, 2900.
(34) Heidrich, D. *Angew. Chem., Int. Ed.* **2002**, *41*, 3208.
(35) Lau, Y. K.; Kebarle, P. *J. Am. Chem. Soc.* **1976**, *98*, 7452.
(36) DeFrees, D. J.; McIver, R. T.; Hehre, W. J. *J. Am. Chem. Soc.* **1977**, *99*, 3853.
(37) Martinsen, D. P.; Buttril, S. E., Jr. *Org. Mass. Spectrom.* **1976**, *11*, 762.
(38) Martinsen, D. P.; Buttril, S. E., Jr. *J. Am. Chem. Soc.* **1978**, *100*, 6559.
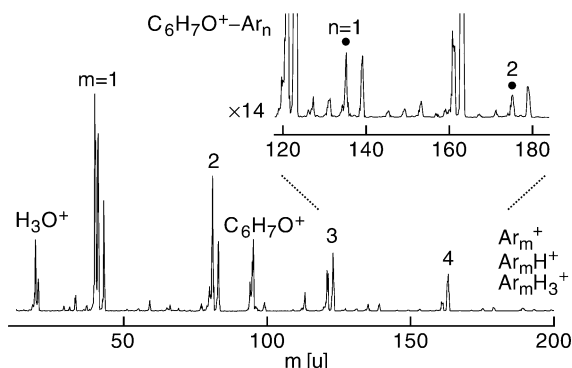(39) Wood, K. V.; Burinsky, D. J.; Cameron, D.; Cooks, R. G. *J. Org. Chem.* **1983**, *48*, 5236.
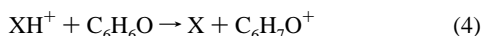
Figure 2. Mass spectrum of the electron ionization source for a coexpansion of 5% H_2 in Ar and phenol vapor at $p_s = 8$ bar. The most intense peaks are assigned to Ar_m^+, Ar_mH^+, and $Ar_mH_3^+$ ($m = 1-4$), protonated phenol ($C_6H_7O^+$), and H_3O^+ (originating from H_2O impurities in the gas inlet system). Part of the spectrum is vertically expanded by a factor of 14 to visualize small peaks, such as the weakly bound $C_6H_7O^+-Ar_n$ clusters (●).
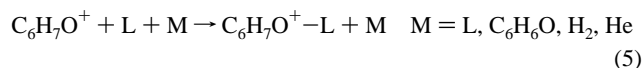
H-bonds between Ar and the OH groups of **1**/**3** and **5**.[23] The intermolecular H–Ar bonds significantly perturb the properties of the intramolecular O–H bonds via H-bonding solvation effects. The lack of detection of *meta* and *ipso* protonation of C_6H_6O confirms that, similar to the liquid phase, the OH group of phenol is a strongly *ortho* and *para* directing and activating substituent also in the gas phase.[23] The main goal of the present study is the characterization of different $C_6H_7O^+-L$ dimers (L = Ne, Ar, N_2) via IRPD and the application of the messenger approach to derive spectroscopic properties of bare oxonium and carbenium ions of $C_6H_7O^+$. The experimental results are complemented by quantum chemical calculations, which provide additional information on both the $C_6H_7O^+$ isomers and the intermolecular interaction in their $C_6H_7O^+-L$ dimers.

2. Experimental and Theoretical Methods

IRPD spectra of mass-selected $C_6H_7O^+-L$ (L = Ne, Ar, N_2) dimers are recorded in a tandem quadrupole mass spectrometer coupled to an ion source and an octopole ion trap.[40] The cluster ion source combines a pulsed molecular beam expansion with electron ionization (EI). The gas mixture, obtained by passing H_2:Ne (ratio 1:20), H_2:Ar (1:20), or H_2:He:N_2 (1:1:20) over a heated phenol sample ($T \approx 360$ K), expands through a pulsed nozzle into a vacuum chamber at stagnation pressures of $p_s = 3-15$ bar. EI of the gas mixture is accomplished by electron beams ($\approx$100 eV) emitted from two tungsten filaments close to the nozzle orifice. Ion–molecule reactions form Brønsted acids XH^+ (e.g., X = H_2, L) in the high-pressure region of the expansion. XH^+ ions protonate phenol via exothermic proton-transfer reactions:[24]

$$XH^+ + C_6H_6O \rightarrow X + C_6H_7O^+ \tag{4}$$

Subsequent three-body association reactions produce weakly bound $C_6H_7O^+-L$ complexes:

$$C_6H_7O^+ + L + M \rightarrow C_6H_7O^+-L + M \quad M = L, C_6H_6O, H_2, He \tag{5}$$

As an example, Figure 2 shows a mass spectrum of the EI ion source, obtained by coexpanding 5% H_2 in Ar and phenol vapor at $p_s = 8$ bar. Major peaks are assigned to Ar_m^+, Ar_mH^+, $Ar_mH_3^+$ ($m = 1-4$), $C_6H_7O^+$, and H_3O^+ (originating from water impurities in the gas inlet system). The vertically expanded inset demonstrates the production of $C_6H_7O^+-Ar_n$ complexes. $C_6H_7O^+-L$ dimers are selected from the skimmed supersonic plasma expansion by an initial quadrupole mass

spectrometer and injected into an octopole ion guide. A tunable IR laser pulse generated by an optical parametric oscillator (OPO) laser system interacts with the mass-selected $C_6H_7O^+-L$ beam in the octopole. Resonant vibrational excitation of $C_6H_7O^+-L$ induces the rupture of the weak intermolecular bond:

$$C_6H_7O^+-L + \nu_{IR} \rightarrow C_6H_7O^+ + L \tag{6}$$
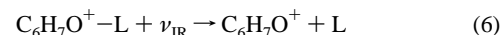
Only this dissociation process is observed upon single-photon IR excitation. The $C_6H_7O^+$ fragment ions are selected by a second quadrupole mass filter and monitored as a function of the laser frequency to obtain the IR action spectrum of $C_6H_7O^+-L$. Frequency calibration, accurate to better than 0.2 cm^{-1}, is accomplished by recording optoacoustic spectra of NH_3 and HDO (using the idler and signal outputs of the OPO laser) simultaneously with the IRPD spectra.[41] All IRPD spectra are linearly normalized for laser intensity variations measured with an InSb detector.

Ab initio and density functional calculations are carried out for all $C_6H_7O^+$ isomers (**1**−**5**) and their complexes with Ne, Ar, and N_2 at the MP2(fc) and B3LYP levels using the 6-311G(2df,2pd) basis set.[42] All coordinates are relaxed during the search for stationary points. Intermolecular dissociation energies (D_e) of $C_6H_7O^+-L$ are corrected for basis set superposition error and fragment relaxation energy.[43,44] Harmonic vibrational frequencies are scaled by a factor of 0.955 (B3LYP). The analysis of the $C_6H_7O^+$ charge distributions is carried out at the MP2 level employing the AIM (atoms-in-molecules) population analysis. The properties of the cis and trans isomers of o/m-$C_6H_7O^+$ (as well as their o/m-$C_6H_7O^+-L$ dimers) relevant for the present work are rather similar. Consequently, if not stated otherwise, they are discussed as single structures denoted as **1** (o-$C_6H_7O^+$) and **2** (m-$C_6H_7O^+$).

3. Results and Discussion

3.1. Theoretical Results. Table 1 summarizes relevant properties of x-$C_6H_7O^+$. Only σ-complexes (C or O protonation of phenol, **1**−**5**) are considered, because π-complexes of aromatic molecules with small electrophiles (such as H^+) are saddle points on the AH^+ potential.[34] In agreement with previous MP2 and B3LYP calculations,[23,31−33] the relative stabilization energies, E_{rel} (given with respect to p-$C_6H_7O^+$), vary in the order **3** < **1** < **5** < **2** < **4** at the MP2 level, and the stabilities of **5** and **2** are reversed at the B3LYP level (Figure 3). As reported previously,[32] the PA of phenol for protonation in the *para* position calculated with the B3LYP and MP2 methods (PA = 833 and 796 kJ/mol) over- and underestimates the experimental value (PA = 816−817 kJ/mol).[35,45] Differences between E_{rel} calculated using the 6-311G(2df,2pd) and the 6-31G* basis[23] are small for all carbenium isomers **1**−**4** (<5 kJ/mol). In contrast, E_{rel} of the oxonium ion **5** is remarkably lower using the larger 6-311G(2df,2pd) basis (by 16 kJ/mol at MP2 and

(40) Dopfer, O. *Int. Rev. Phys. Chem.* **2003**, *22*, 437.

(41) Guelachvili, G.; Rao, K. N. *Handbook of Infrared Standards*; Academic Press: London, 1993.
(42) Frisch, M. J.; Trucks, G. W.; Schlegel, H. B.; Scuseria, G. E.; Robb, M. A.; Cheeseman, J. R.; Zakrzewski, V. G.; Montgomery, J. A., Jr.; Stratmann, R. E.; Burant, J. C.; Dapprich, S.; Millam, J. M.; Daniels, A. D.; Kudin, K. N.; Strain, M. C.; Farkas, O.; Tomasi, J.; Barone, V.; Cossi, M.; Cammi, R.; Mennucci, B.; Pomelli, C.; Adamo, C.; Clifford, S.; Ochterski, J.; Petersson, G. A.; Ayala, P. Y.; Cui, Q.; Morokuma, K.; Malick, D. K.; Rabuck, A. D.; Raghavachari, K.; Foresman, J. B.; Cioslowski, J.; Ortiz, J. V.; Stefanov, B. B.; Liu, G.; Liashenko, A.; Piskorz, P.; Komaromi, I.; Gomperts, R.; Martin, R. L.; Fox, D. J.; Keith, T.; Al-Laham, M. A.; Peng, C. Y.; Nanayakkara, A.; Gonzalez, C.; Challacombe, M.; Gill, P. M. W.; Johnson, B. G.; Chen, W.; Wong, M. W.; Andres, J. L.; Head-Gordon, M.; Replogle, E. S.; Pople, J. A. *Gaussian 98*, revision A.7; Gaussian, Inc.: Pittsburgh, PA, 1998.
(43) Boys, S. F.; Bernardi, F. *Mol. Phys.* **1970**, *19*, 553.
(44) Chalasinski, G.; Szczesniak, M. M. *Chem. Rev.* **1994**, *94*, 1.
(45) Hunter, E. P. L.; Lias, S. G. *J. Phys. Chem. Ref. Data* **1998**, *27*, 413.

Table 1. Selected Properties of Possible C$_6$H$_7$O$^+$ Isomers: Relative Energies Corrected for Zero-Point Energy (E_{rel}), O−H Separations (R_{OH}), and O−H (ν_{OH}) and Aliphatic C−H (ν_{CH}) Stretch Frequencies^a Calculated at the MP2/6-311G(2df,2pd) and B3LYP/6-311G(2df,2pd) Levels

	MP2		B3LYP			
ion	E_{rel} [kJ/mol]^b	R_{OH} [Å]	E_{rel} [kJ/mol]	R_{OH} [Å]	ν_{OH} [cm^{-1}]^c	ν_{CH} (sp^3) [cm^{-1}]^c
1a	13.46	0.970	11.03	0.970	3563.6 (215)	2858.2 (39) 2868.2 (17)
1b	18.16	0.969	17.16	0.969	3575.0 (220)	2850.0 (23) 2866.2 (12)
2a	66.52	0.964	65.43	0.965	3630.4 (157)	2802.8 (26) 2811.6 (64)
2b	64.44	0.965	62.72	0.965	3625.5 (152)	2806.6 (23) 2814.0 (57)
3	0	0.970	0	0.970	3566.3 (223)	2842.5 (35) 2843.4 (11)
4	119.65	0.964	125.97	0.965	3626.9 (111)	2561.5 (110)
5	46.54	0.974	77.10	0.974	3555.8 (305) 3479.7 (245)	−

^{a} Harmonic frequencies are scaled by 0.955. ^{b} E_{rel} values determined at the MP2 level are corrected using the zero-point energy calculated at the B3LYP level. ^{c} IR intensities (I_{OH} and I_{CH} in km/mol) are given in parentheses.
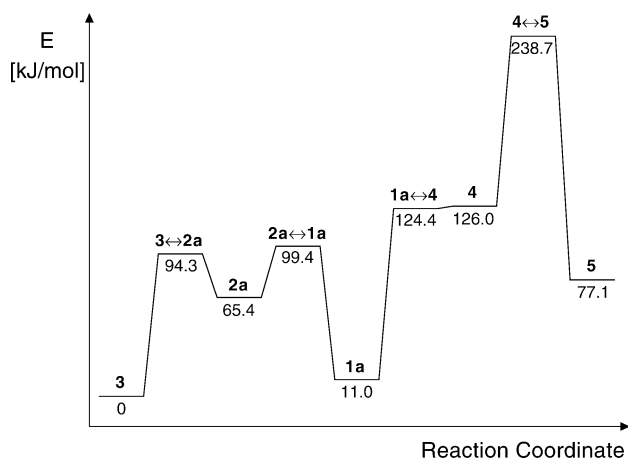

Figure 3. Salient parts of the potential energy surface of C$_6$H$_7$O$^+$ calculated at the B3LYP/6-311G(2df,2pd) level. Relative energies (E_{rel} in kJ/mol, given with respect to **3**) are corrected for zero-point energy (ZPE). Transition states for proton migration from structure **x** to **y** are denoted as **x** ↔ **y**. Without ZPE correction, structure **4** corresponds to a local minimum on the PES.

B3LYP),[23] yielding a better match between the experimental (E_{rel} = 63 kJ/mol)[36] and B3LYP energies (E_{rel} = 77 kJ/mol).

Figure 3 illustrates part of the potential energy surface (PES) of C$_6$H$_7$O$^+$ (B3LYP). Transition states for proton migration from structure **x** to structure **y** are denoted as **x** ↔ **y** (**x**, **y** = **1**−**5**). The cis isomers **1b** and **2b** as well as their transition states toward **3** and **4** are not considered, because E_{rel} values of cis and trans structures are very similar (Table 1).[32] Vibrational analysis for **1**−**5** confirms their identification as minima on the PES. After correction for zero-point energy, however, E_{rel} of **4** exceeds E_{rel} of **1a** ↔ **4**, suggesting that i-C$_6$H$_7$O$^+$ (**4**) is metastable with respect to proton migration toward o-C$_6$H$_7$O$^+$ (**1**). On the other hand, isomerization of m-C$_6$H$_7$O$^+$ (**2**) toward the more stable carbenium ions **1** and **3** is associated with barriers on the order of $V \approx$ 30 kJ/mol, and isomerization of **5** into **1**−**4** requires an even larger barrier, $V(5 \to 4) \approx$ 160 kJ/mol.

Certain C$_6$H$_7$O$^+$ ions feature very different properties of the O−H bond(s), such as bond lengths (R_{OH}), stretching frequencies

(ν_{OH}), and corresponding IR intensities (I_{OH}).[23,32] The B3LYP results are summarized in Table 1. Briefly, the C$_6$H$_7$O$^+$ isomers can be classified into three groups according to the properties of their O−H bonds: the oxonium ion (**5**), the *ortho* and *para* protonated carbenium ions (**1/3**), and the *meta* and *ipso* protonated carbenium ions (**2/4**). The strength of the O−H bonds decreases in the order **2/4** > **1/3** > **5**, and their acidity increases accordingly. These trends are apparent in the calculated R_{OH} and ν_{OH} values (Table 1): ν_{OH} decreases along the series **2/4** > **1/3** > **5**, and R_{OH} shows the reversed trend. Figure 4 compares IR stick spectra of **1**−**5** (B3LYP). Again, ν_{OH} and I_{OH} values of **1** and **3**, and also of **2** and **4**, are very similar. For the oxonium ion **5**, the two ν_{OH} bands represent the symmetric and antisymmetric combinations of the two local O−H oscillators, $\nu_{OH,s}$ and $\nu_{OH,as}$. Their center frequency, $\nu_{OH,av}$, corresponds to a measure of the O−H bond strength in **5**. In addition to ν_{OH}, C−H stretch modes (ν_{CH}) are also included in Figure 4 and Table 1. In the aromatic C−H stretch range (ν > 3000 cm^{-1}), ν_{CH} modes with sp^2 hybridization of the C atoms are very weak and occur for all considered ions **1**−**5** between 3022 and 3069 cm^{-1}. The carbenium isomers **1**−**4** feature more intense aliphatic ν_{CH} vibrations (sp^3 hybridization of the protonated C atom) in the range ν < 3000 cm^{-1}. In general, the predicted ν_{CH} (sp^3) frequency differences between **1** and **3**, and **2** and **4**, are larger than those for ν_{OH}. Noteworthy, ν_{CH} (sp^3) of **2** are markedly shifted from ν_{CH} (sp^3) of **4**, indicating that, in contrast to the O−H stretch range, **2** and **4** can readily be distinguished in the C−H stretch range.

H-bonding of Ne, Ar, or N$_2$ to the acidic OH groups of **1**−**5** induces significant changes in the O−H bond properties of the bare C$_6$H$_7$O$^+$ isomers. Relevant inter- and intramolecular parameters of C$_6$H$_7$O$^+$−Ar and C$_6$H$_7$O$^+$−N$_2$ (B3LYP) are summarized in Tables 2 and 3, respectively.[46] The O−H−L bonds in the H-bound dimers, denoted as (**1**−**5**)−**L(H)**, are slightly nonlinear (178° < φ < 167°). The acidity order of the intramolecular O−H bond(s) in C$_6$H$_7$O$^+$, **5** > **1/3** > **2/4**, is correlated with the strength of the intermolecular OH−L bonds in the corresponding H-bound dimers. For example, dimers of the oxonium ion **5**−**L(H)** feature a larger dissociation energy (D_e), a shorter intermolecular separation (R_{HL}), a larger intermolecular H−L stretch frequency (ν_s), and a larger complexation-induced R_{OH} elongation (ΔR_{OH}) than dimers of the carbenium ions (**1**−**4**)−**L(H)**. These effects are larger in C$_6$H$_7$O$^+$−N$_2$ as compared to C$_6$H$_7$O$^+$−Ar, because of the stronger intermolecular interaction in the former complexes. Figure 4 compares the IR stick spectra calculated for the H-bound dimers of all C$_6$H$_7$O$^+$ isomers with Ar and N$_2$, (**1**−**5**)−**Ar(H)** and (**1**−**5**)−**N$_2$(H)**. In all cases, the H-bound ν_{OH} modes experience a complexation-induced shift to lower frequencies (red shifts $\Delta\nu_{OH}$ up to 11%), and their IR intensities are enhanced (up to 600%). The acidity order of the OH groups of the different C$_6$H$_7$O$^+$ ions can be clearly recognized in Figure 4. For example, the most pronounced red shifts are obtained for $\nu_{OH,s}$ of **5**, which transforms to the bound ν_{OH} vibration ($\nu_{OH,b}$) upon H-bonding. Because of the similar intermolecular interaction in **1**−**L(H)** and **3**−**L(H)**, and also in **2**−**L(H)** and **4**−**L(H)**, the ν_{OH} bands of these dimers occur at approximately the same frequencies. Consequently, it is difficult to discriminate

(46) As B3LYP calculations of charged complexes containing Ne are not reliable,[67] computational results of the C$_6$H$_7$O$^+$−Ne dimers are not discussed further.
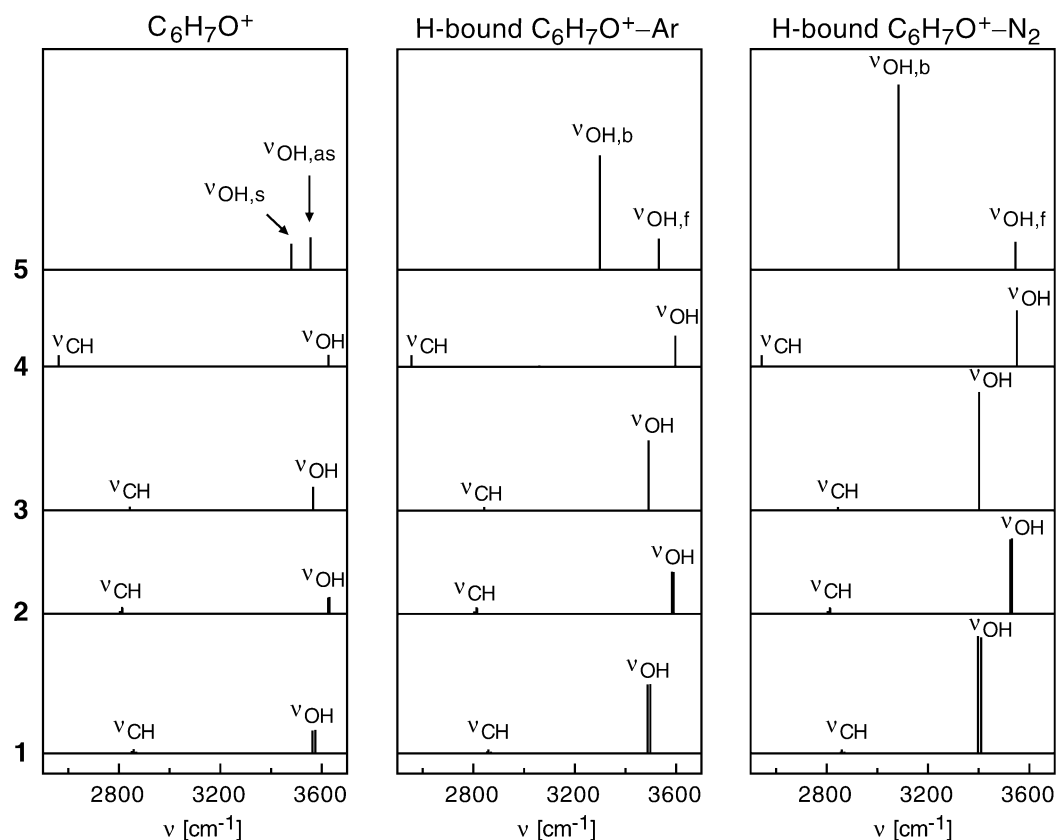
Figure 4. IR stick spectra of $C_6H_7O^+$, H-bound $C_6H_7O^+$–Ar, and H-bound $C_6H_7O^+$–N$_2$ calculated for all possible $C_6H_7O^+$ isomers: the carbenium isomers **1**−**4** and the oxonium ion **5** (B3LYP, Tables 1−3). Trans and cis isomers of o-$C_6H_7O^+$ (**1a/b**) and m-$C_6H_7O^+$ (**2a/b**) are plotted together as **1** and **2**, respectively. Aliphatic C−H (sp^3) and O−H stretch vibrations are indicated as ν_{CH} and ν_{OH}. The symmetric and antisymmetric combinations of the two local O−H oscillators of **5** are designated as $\nu_{OH,s}$ and $\nu_{OH,as}$. The bound and free O−H stretch modes of **5**−**L(H)** are denoted $\nu_{OH,b}$ and $\nu_{OH,f}$, respectively. Aromatic C−H (sp^2) stretch modes between 3020 and 3070 cm^{-1} are not visible in the simulations because of their low calculated IR intensities.

Table 2. Selected Parameters of the Intermolecular H−Ar and Intramolecular O−H Bonds of H-Bound $C_6H_7O^+$–Ar Isomers Calculated at the B3LYP/6-311G(2df,2pd) Level: Dissociation Energies (D_e in kJ/mol), H−Ar Distances (R_{HAr} in Å), O−H−Ar Angles (φ), H−Ar Stretch Frequencies (ν_s in cm^{-1}), Complexation-Induced O−H Bond Length Changes (ΔR_{OH} in Å), O−H and Aliphatic C−H Stretch Frequencies[a] (ν_{OH} and ν_{CH} in cm^{-1}), and IR Intensities (I_{OH} and I_{CH} in km/mol)

	1a−Ar(H)	1b−Ar(H)	2a−Ar(H)	2b−Ar(H)	3−Ar(H)	4−Ar(H)	5−Ar(H)
D_e	5.29	5.77	4.00	3.95	5.66[b]	3.34	12.25[c]
R_{HAr}	2.391	2.387	2.513	2.497	2.394	2.511	2.167
φ	168°	168°	175°	172°	167°	177°	178°
ν_s	65.7	67.8	54.7	55.6	65.3	65.3	108.6
ΔR_{OH}	0.004	0.004	0.002	0.002	0.004	0.002	0.011
							−0.001
ν_{OH}	3487.1	3498.4	3590.3	3583.7	3491.2	3596.8	3299.6
							3532.4
I_{OH}	647	652	395	398	659	293	1076/293
ν_{CH} (sp^3)	2859.3	2853.3	2802.8	2806.8	2842.7	2555.1	
	2869.2	2869.4	2811.8	2814.3	2843.7		
I_{CH}	38/16	20/11	25/64	22/55	34/11	108	

[a] Harmonic frequencies are scaled by 0.955. [b] D_e = 7.57 kJ/mol at the MP2/6-311G(2df,2pd) level. [c] D_e = 14.14 kJ/mol at the MP2/6-311G(2df,2pd) level.

between **1**−**L(H)** and **3**−**L(H)**, and also between **2**−**L(H)** and **4**−**L(H)**, in the O−H stretch range. In contrast to ν_{OH}, H-bonding with Ar and N$_2$ does not significantly affect the aliphatic ν_{CH} (sp^3) modes of **1**−**4**. Thus, as discussed for ν_{CH} (sp^3) of bare **1**−**4**, a more definitive discrimination between the carbenium isomers is eventually possible in the C−H stretch range.

3.2. Experimental Results. Figure 5 compares IRPD spectra of $C_6H_7O^+$−Ar recorded under different experimental conditions. The spectra are obtained for stagnation pressures of p_s = 3, 8, and 12 bar and subsequent optimization of all other ion source parameters.[40] The positions, widths, and assignments of

the transitions observed are listed in Table 4. The spectrum in trace (a) was discussed in detail in ref 23, and only the salient results are briefly reviewed. On the basis of band profiles, complexation-induced band shifts, and the comparison with quantum chemical calculations, peaks A$_1$ and A$_2$ at 3534 and 3329 cm^{-1} were assigned to the free and bound O−H stretch vibrations ($\nu_{OH,f}$ and $\nu_{OH,b}$) of **5**−**Ar(H)**.[23] Similarly, peak B$_1$ at 3493 cm^{-1} was attributed to ν_{OH} of **1/3**−**Ar(H)**.[23] The calculated frequencies of A$_1$, A$_2$, and B$_1$ (3532, 3300, and ≈3490 cm^{-1}, Table 2) compare favorably with the corresponding experimental values (3534, 3329, and 3493 cm^{-1}, Table 4) and support the given assignment.

Table 3. Selected Parameters of the Intermolecular H−N and Intramolecular O−H Bonds of H-Bound C$_6$H$_7$O$^+$−N$_2$ Isomers Calculated at the B3LYP/6-311G(2df,2pd) Level: Dissociation Energies (D_e in kJ/mol), H−N Distances (R_{HN} in Å), O−H−N Angles (φ), H−N Stretch Frequencies (ν_s in cm^{-1}), Complexation-Induced O−H Bond Length Changes (ΔR_{OH} in Å), O−H and Aliphatic C−H Stretch Frequencies^a (ν_{OH} and ν_{CH} in cm^{-1}), and IR Intensities (I_{OH} and I_{CH} in km/mol)

	1a–N$_2$(H)	1b–N$_2$(H)	2a–N$_2$(H)	2b–N$_2$(H)	3–N$_2$(H)	4–N$_2$(H)	5–N$_2$(H)
D_e	18.10	18.75	14.52	14.21	18.51^b	12.82	32.90^c
R_{HN}	1.977	1.979	2.068	2.065	1.980	2.085	1.774
φ	169°	168°	170°	169°	169°	177°	176°
ν_s	111.3	111.1	96.6	96.4	111.4	87.3	160.0
ΔR_{OH}	0.009	0.009	0.005	0.005	0.008	0.004	0.023 −0.002
ν_{OH}	3396.6	3410.1	3530.8	3524.8	3401.6	3550.9	3083.9 3544.8
I_{OH}	1100	1088	709	699	1112	530	1739/260
ν_{CH} (sp^3)	2860.1 2870.3	2855.9 2872.3	2803.5 2812.1	2807.0 2814.4	2844.3 2845.6	2543.6	
I_{CH}	37/15	17/9	25/62	21/53	32/10	109	

^{a} Harmonic frequencies are scaled by 0.955. ^{b} D_e = 21.63 kJ/mol at the MP2/6-311G(2df,2pd) level. ^{c} D_e = 35.82 kJ/mol at the MP2/6-311G(2df,2pd) level.
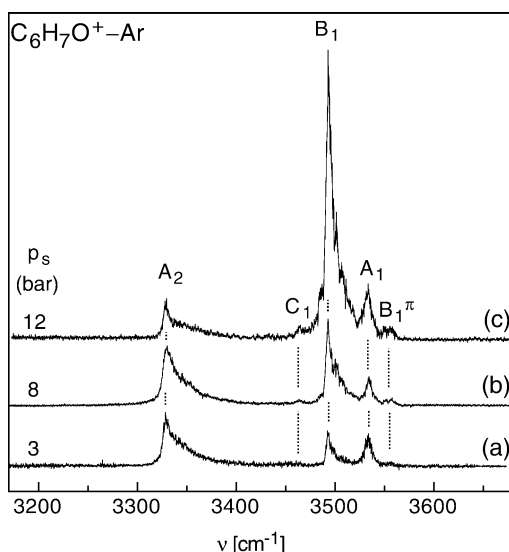

Figure 5. IRPD spectra of C$_6$H$_7$O$^+$−Ar between 3170 and 3680 cm^{-1} recorded under different experimental conditions. Transitions marked with A$_i$, B$_i$, and C$_i$ originate from O-C$_6$H$_7$O$^+$−Ar, o/p-C$_6$H$_7$O$^+$−Ar, and ^{13}C^{12}C$_5$H$_6$O$^+$−Ar, respectively (Table 4). Signal optimization using higher stagnation pressures (p_s) clearly enhances the relative abundance of o/p-C$_6$H$_7$O$^+$−Ar (**1/3−Ar**, bands B$_1$/B$_1^\pi$) with respect to O-C$_6$H$_7$O$^+$−Ar (**5−Ar**, bands A$_{1/2}$).

Although all spectra in Figure 5 are similar with respect to peak positions, the relative intensities of several bands vary drastically. In particular, the conditions employed for spectrum (c) as compared to those of (a) enhance the production of **1/3−Ar(H)** over **5−Ar(H)** by a factor of ≈5, thus confirming that transitions A$_{1/2}$ and B$_1$ clearly arise from different carriers. Apparently, the widths of A$_2$ and B$_1$ decrease for increasing p_s (Table 4), indicating that the complexes are produced with less internal energy at higher p_s. In addition to the bands A$_1$, A$_2$, and B$_1$ observed in spectrum (a), new features are clearly identified in spectra (b) and (c). The carrier(s) of these peaks must be different from **5−Ar(H)**, because the relative intensity of this isomer is reduced at higher p_s. By comparison with the IRPD spectrum of phenol$^+$−Ar,^{30,47} band C$_1$ at 3464 cm^{-1} is readily assigned to possible ^{13}C isotopomers of H-bound phenol$^+$−Ar, ^{13}C^{12}C$_5$H$_6$O$^+$−Ar = **^{13}C−Ar(H)**, which contaminate the mass channel of C$_6$H$_7$O$^+$−Ar (^{12}C$_6$H$_7$O$^+$−Ar). From the mass spectrum in Figure 2, the ^{13}C−Ar contamination of the m = 135 u channel is estimated as 2−3%. As expected, the position of C$_1$ matches the ν_{OH} frequency of H-bound phenol$^+$−Ar (^{12}C$_6$H$_6$O$^+$−Ar), demonstrating that ^{12}C → ^{13}C substitutions have only minor effects on the O−H bond of phenol$^+$.^{30,47} In addition to C$_1$, a symmetric peak centered at 3554 cm^{-1} (B$_1^\pi$) is observed in Figure 5, and its intensity is correlated with that of B$_1$ assigned to ν_{OH} of **1/3−Ar(H)**. Hence, B$_1^\pi$ is assigned to ν_{OH} of the less stable π-bound Ar dimers, **1/3−Ar(π)**.

The spectral detection of the **1/3−Ar(π)** local minimum is expected according to the following arguments. The ν_{OH} band of the local π-bound minimum was also observed in the IRPD spectrum of phenol$^+$−Ar.$^{30,47−49}$ The small difference in the binding energy of H-bound and π-bound phenol$^+$−Ar, ΔD_e ≈ 3.1 kJ/mol (MP2/6-311G(2df,2pd)), was invoked to explain the efficient production of the π-bound local minimum in addition to the H-bound global minimum.^{48} Calculations at the same level of theory predict an even smaller binding energy difference of ΔD_e ≈ 1.7 kJ/mol between **3−Ar(H)** and **3−Ar(π)**. Moreover, I_{OH} values calculated at the B3LYP/6-31G* level are similar for H-bound phenol$^+$−Ar and **3−Ar(H)**, and also for π-bound phenol$^+$−Ar and **3−Ar(π)** (I_{OH} ≈ 500 and 200 km/mol, respectively). Consequently, the efficient production and IR detection of **1/3−Ar(π)** in Figure 5 is not surprising. Moreover, B$_1^\pi$ features a symmetric peak profile, as expected for a π-bound dimer.^{48} In contrast to **1/3−Ar(π)**, **5−Ar(π)** is not detected in the IRPD spectrum, probably because of the larger difference in the Ar binding energies between **5−Ar(H)** and **5−Ar(π)** and/or low isomerization barriers from **5−Ar(π)** toward **5−Ar(H)**. In fact, all efforts to calculate the structure of **5−Ar(π)** at the MP2 level failed, because all chosen π-bound starting geometries converged to the most stable H-bound structure. Finally, complexes of **2** and **4** are not observed in Figure 5. These ions are considerably less stable than **3** and **1**, and their production in the EI ion source is significantly suppressed. On the other hand, the large isomerization barrier separating **5** from the carbenium ions, $V(\mathbf{5} → \mathbf{4})$ ≈ 160 kJ/mol, accounts for the efficient production of **5−Ar** (section 4).^{23,32}

Figure 6 compares the IRPD spectra of C$_6$H$_7$O$^+$−L (L = Ne, Ar, N$_2$) between 2650 and 3700 cm^{-1} (Table 4). In addition

(47) Solcà, N.; Dopfer, O. *J. Mol. Struct.* **2001**, *563−564*, 241.

(48) Solcà, N.; Dopfer, O. *Chem. Phys. Lett.* **2000**, *325*, 354.
(49) Solcà, N.; Dopfer, O. *Chem. Phys. Lett.* **2003**, *369*, 68.

Table 4. Band Maxima (cm^{-1}), Widths (cm^{-1}, fwhm, in Parentheses), and Assignments of Vibrational Transitions Observed in the IRPD Spectra of Protonated Phenol Complexes (x-C$_6$H$_7$O$^+$–L with L = Ne, Ar, N$_2$)^a

band	position	assignment	isomer	band	position	assignment	isomer
A$_1$	3552 (10)	$\nu_{OH,f}$	**5–Ne(H)**^{b}	B$_5$	3069 (22)	ν_{CH} (sp^2)	**1/3–Ar(H)**^{e}
B$_1$	3552 (10)	ν_{OH}	**1/3–Ne(H)**^{b}	B$_3$	2877 (12)	ν_{CH} (sp^3)	**1/3–Ar(H)**
A$_2$	3477 (10)	$\nu_{OH,b}$	**5–Ne(H)**	B$_2$	2864 (9)	ν_{CH} (sp^3)	**1/3–Ar(H)**
B$_3$	2877 (10)	ν_{CH} (sp^3)	**1/3–Ne(H)**	A$_1$	3543 (12)	$\nu_{OH,f}$	**5–N$_2$(H)**
B$_2$	2865 (10)	ν_{CH} (sp^3)	**1/3–Ne(H)**	B$_1$	3408 (6)	ν_{OH}	**1/3–N$_2$(H)**
B$_1^\pi$	3554 (13)	ν_{OH}	**1/3–Ar(π)**	C$_1$	3365 (4)	ν_{OH}	**^{13}C–N$_2$(H)**
A$_1$	3534 (9)	$\nu_{OH,f}$	**5–Ar(H)**	A$_3$	3252 (34)^f	$\nu_{OH,b} + \nu_s$	**5–N$_2$(H)**
B$_1$	3493 (12)^c	ν_{OH}	**1/3–Ar(H)**	A$_2$	3073 (36)^f	$\nu_{OH,b}$	**5–N$_2$(H)**
C$_1$	3464 (10)	ν_{OH}	**^{13}C–Ar(H)**	B$_3$	2877 (12)	ν_{CH} (sp^3)	**1/3–N$_2$(H)**
A$_2$	3329 (23)^d	$\nu_{OH,b}$	**5–Ar(H)**	B$_2$	2865 (10)	ν_{CH} (sp^3)	**1/3–N$_2$(H)**
B$_4$	3046 (16)	ν_{CH} (sp^2)	**1/3–Ar(H)**^{e}				

^{a} Oxonium and carbenium isomers of C$_6$H$_7$O$^+$ are denoted as **5** (bands A$_i$) and **1/3** (bands B$_i$). Transitions originating from the contamination ^{13}C^{12}C$_5$H$_6$O$^+$–L are denoted as **^{13}C–L** (band C$_1$). All peaks are assigned to H-bound complexes (H, in parentheses), with the exception of B$_1^\pi$ assigned to π-bound o/p-C$_6$H$_7$O$^+$–Ar. ^{b} Both **5–Ne(H)** and **1/3–Ne(H)** isomers contribute to this band (see text). ^{c} The width of this peak decreases to 10 cm^{-1} for p_s = 12 bar (Figure 5). ^{d} The width of this peak decreases from 23 to 18 and 15 cm^{-1} for p_s = 3, 8, and 12 bar (Figure 5). ^{e} Part of the signal may originate from the H-bound O-C$_6$H$_7$O$^+$–Ar isomer (see text). ^{f} A$_2$ and A$_3$ probably arise from transitions of the type $\nu_{OH,b} + \nu_x \leftarrow \nu_x$ and $\nu_{OH,b} + \nu_s + \nu_x \leftarrow \nu_x$.
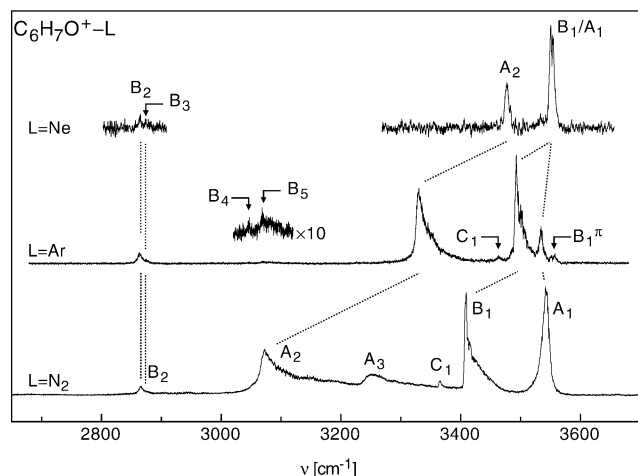

Figure 6. IRPD spectra of C$_6$H$_7$O$^+$–L (L = Ne, Ar, N$_2$) between 2650 and 3700 cm^{-1}. Transitions marked with A$_i$ and B$_i$ are assigned to the O-C$_6$H$_7$O$^+$–L (**5–L**) and the o/p-C$_6$H$_7$O$^+$–L (**1/3–L**) isomers, respectively (Table 4). The ν_{OH} bands of ^{13}C^{12}C$_5$H$_6$O$^+$–L (**^{13}C–L**) are labeled with C$_1$. With the exception of B$_1^\pi$, which is assigned to π-bound o/p-C$_6$H$_7$O$^+$–Ar, all peaks are assigned to H-bound C$_6$H$_7$O$^+$–L dimers. The spectra have been recorded after optimizing the ion signal at p_s = 6 (L = N$_2$), 8 (L = Ar), and 15 bar (L = Ne).

to the ν_{OH} transitions discussed above, the C$_6$H$_7$O$^+$–Ar spectrum features peaks in the C–H stretch range at 2864 (B$_2$), 2877 (B$_3$), 3046 (B$_4$), and 3069 cm^{-1} (B$_5$). B$_2$ and B$_3$ occur in the aliphatic C–H stretch range and must be assigned to a carbenium isomer of C$_6$H$_7$O$^+$. Resonant coupling between the two equivalent aliphatic C–H bonds in **1** and **3** gives rise to symmetric $\nu_{CH,s}$ (sp^3) and antisymmetric $\nu_{CH,as}$ (sp^3) normal modes. Thus, possible assignments of B$_2$ and B$_3$ include $\nu_{CH,s}$ and $\nu_{CH,as}$ of **1–Ar** and/or **3–Ar**, or $\nu_{CH,s}$ of **1–Ar** and **3–Ar**, respectively. As it is difficult to discriminate between both possibilities (Table 2), B$_{2/3}$ are assigned less specifically to ν_{CH} (sp^3) of **1/3–Ar(H)**. Because of the much smaller production of **1/3–Ar(π)**, the contribution of this isomer to these bands can be neglected. As the C–H stretch modes are essentially unperturbed upon OH-bonding of C$_6$H$_7$O$^+$ with different L, the nearly unshifted B$_{2/3}$ bands of the Ne and N$_2$ complexes (Figure 6) are readily identified also as ν_{CH} (sp^3).

At least two bands are observed for C$_6$H$_7$O$^+$–Ar in the aromatic C–H stretch range. B$_4$ and B$_5$ at 3046 and 3069 cm^{-1} are tentatively assigned to ν_{CH} (sp^2) of **1/3–Ar(H)**. Although **5–Ar(H)** may significantly contribute to B$_{4/5}$, this option is less

probable, because I_{CH} (sp^2) values calculated for **1/3–Ar(H)** are larger (by a factor of $\approx$1.5) and the relative abundance of **1/3–Ar(H)** as compared to **5–Ar(H)** is estimated to be $\approx$2:1 in the spectrum of Figure 6. The given assignment agrees with the B3LYP calculations, which predict ν_{CH} (sp^2) of **1/3–Ar(H)** between 3041 and 3069 cm^{-1}. Moreover, the calculated ratio of I_{CH} (sp^2) and I_{CH} (sp^3) is $\approx$1:5, also compatible with the experiment ($\approx$1:3). The ν_{CH} (sp^2) transitions are not identified for C$_6$H$_7$O$^+$–Ne and C$_6$H$_7$O$^+$–N$_2$, because they are below the noise level (Ne) or hidden by the strong A$_2$ peak (N$_2$).

The A$_2$ peak in the C$_6$H$_7$O$^+$–Ar spectrum is attributed to the bound O–H stretch vibration of **5–Ar(H)**. Replacing Ar by N$_2$ induces a considerable red shift, $\Delta\nu_{OH,b}$ [Ar → N$_2$], as a consequence of the stronger H-bond (Section 3.1). Thus, band A$_2$ at 3073 cm^{-1} in the C$_6$H$_7$O$^+$–N$_2$ spectrum is identified as $\nu_{OH,b}$ of **5–N$_2$(H)**. This assignment is confirmed by the favorable comparison between experimental and calculated $\Delta\nu_{OH,b}$ [Ar → N$_2$] shifts of −256 and −216 cm^{-1}, respectively. Moreover, band A$_2$ of C$_6$H$_7$O$^+$–N$_2$ is considerably shaded to the blue, consistent with an assignment to a bound O–H stretch mode.[23,29,48] On the other hand, the free O–H stretch band of **5–N$_2$(H)** is expected with a rather symmetric profile close to the corresponding vibration of **5–Ar(H)**. Hence, peak A$_1$ at 3543 cm^{-1} is attributed to $\nu_{OH,f}$ of **5–N$_2$(H)**. The experimental $\Delta\nu_{OH,f}$ [Ar → N$_2$] shift (9 cm^{-1}) is similar to the calculated value (12 cm^{-1}). The third intense, blue shaded peak in the C$_6$H$_7$O$^+$–N$_2$ spectrum at 3408 cm^{-1} (B$_1$) is assigned to ν_{OH} of **1/3–N$_2$(H)**. The detection of B$_{213}$ for C$_6$H$_7$O$^+$–N$_2$ indicates the substantial abundance of the **1/3–N$_2$(H)** isomer. Also for B$_1$, good agreement between experimental and calculated $\Delta\nu_{OH}$ [Ar → N$_2$] is noticed (−85 and −94 cm^{-1}). Two additional weaker peaks (A$_3$ and C$_1$) are observed in the O–H stretch range of the C$_6$H$_7$O$^+$–N$_2$ spectrum. The relatively large and similar widths of A$_2$ and A$_3$ (fwhm = 36 and 34 cm^{-1}) suggest that both of them originate from the same carrier, that is, **5–N$_2$(H)**. Band A$_3$ is ascribed to the combination band $\nu_{OH,b}$ + ν_s of **5–N$_2$(H)**, where ν_s is the intermolecular OH–N stretch vibration. Such combination bands were observed in the IR spectra of related H-bound dimers, such as SiOH$^+$–N$_2$[29] and C$_6$H$_5$OH$^+$–N$_2$.[48] The derived ν_s frequency of **5–N$_2$(H)** in the $\nu_{OH,b}$ = 1 excited state, 179 cm^{-1}, is slightly larger than that calculated for the ground state (160 cm^{-1}, Table 3), probably

because of the increase in the OH–N interaction induced by excitation of the O–H donor stretch.[26] Finally, peak C_1 at 3365 cm^{-1} is attributed to ν_{OH} of H-bound $^{13}C^{12}C_5H_6O^+-N_2$, **$^{13}C-N_2(H)$**, which contaminates the $m = 123$ u mass channel of $^{12}C_6H_7O^+-N_2$. Similar to $C_6H_7O^+-Ar$, the position of C_1 matches ν_{OH} of H-bound phenol$^+-N_2$.[30,48]

The calculated binding energy of **$5-N_2(H)$**, $D_e = 35.82$ kJ/mol (=2994 cm^{-1}) and 32.90 kJ/mol (=2750 cm^{-1}) at the MP2 and B3LYP levels, is close to the energy of its O–H stretch fundamentals ($\nu_{OH,f} = 3543$ cm^{-1} and $\nu_{OH,b} = 3073$ cm^{-1}). If the calculations somewhat underestimate the binding energy, some amount of (rovibrational) internal energy prior to IR excitation is necessary to induce single photon IRPD of **$5-N_2(H)$**.[50] In fact, the large total widths of $A_{2/3}$ (>100 cm^{-1}) suggest that the **$5-N_2(H)$** complexes observed in Figure 6 contain a significant amount of internal energy. This conclusion, however, does not hold for the significantly narrower A_1 peak, and the energy of a single IR photon in this range ($\nu_{IR} \approx 3500$ cm^{-1}) seems to be sufficient to cleave the OH–N bond in the ground vibrational state of **$5-N_2(H)$**. Moreover, the (integrated) relative intensity ratio of the $\nu_{OH,b}$ and $\nu_{OH,f}$ bands (≈2) is much smaller than the predicted ratio (≈7, Table 3), again suggesting that the contribution of cold **$5-N_2(H)$** to $A_{2/3}$ is absent. Hence, assuming that A_2 and A_3 arise from sequence transitions of the type $\nu_{OH,b} + \nu_x \leftarrow \nu_x$ and $\nu_{OH,b} + \nu_s + \nu_x \leftarrow \nu_x$ (where ν_x are probably low-frequency vibrations),[24,51] one can conclude that the dissociation energy of **$5-N_2(H)$** is bracketed by A_3 and A_1, leading to $D_0 \approx 41 \pm 2$ kJ/mol.

At first glance, it is not obvious whether the H- or π-bound structure is more stable for both **$1/3-Ne$** and **$5-Ne$**. On the basis of the following argument, the H-bound isomers are concluded to be the global minima of the intermolecular PES of the Ne dimers (similar to the Ar and N_2 complexes). Systematic complexation-induced frequency shifts of phenol^+-Rg complexes (Rg = He, Ne, Ar)[30] show that the H-bound structure is the global minimum of phenol^+-Ne. As discussed above, the H-bond strength in OH-bound complexes scales, for a given Rg ligand, with the acidity of the OH donor group. In contrast, the strengths of the π-bonds in phenol^+-Ne, **$1/3-Ne(\pi)$**, and **$5-Ne(\pi)$** are expected to be similar.[21] The O–H bonds of **5** are certainly more acidic than that of phenol$^+$, whereas the acidities of **1/3** and phenol$^+$ are comparable (vide infra). Thus, **$1/3-Ne(H)$** and **$5-Ne(H)$** are concluded to be the most stable structures on their PES and expected to dominate the IRPD spectrum of $C_6H_7O^+-Ne$.

The IRPD spectrum of $C_6H_7O^+-Ne$ displays two peaks in the O–H stretch range. Transition A_2 at 3477 cm^{-1} is assigned to $\nu_{OH,b}$ of **$5-Ne(H)$**. The H-bonds in the Ne dimers are considerably weaker than those in the Ar dimers, implying that A_2 of **$5-Ne(H)$** is shifted to higher frequencies as compared to A_2 of **$5-Ar(H)$**. As A_2 of **$5-Ne(H)$** occurs at a lower frequency than ν_{OH} of **$1/3-Ar(H)$** (B_1), an assignment to ν_{OH} of **$1/3-Ne(H)$** can be excluded. The intensity ratio of $\nu_{OH,b}$ and $\nu_{OH,f}$ (A_2 and A_1) of **$5-Ne(H)$** is expected to be only slightly larger than that of bare **5** ($\sim$1:1, Figure 4, Table 1), because of the weak perturbation by the H-bound Ne ligand. Thus, a considerable fraction of the signal at 3552 cm^{-1} is attributed to

$\nu_{OH,f}$ of **$5-Ne(H)$** (A_1). On the other hand, part of this signal must also arise from ν_{OH} of **$1/3-Ne(H)$** (B_1). First, this band should be observed in the O–H stretch range, because the detection of $B_{2/3}$ in the C–H stretch range implies a substantial abundance of **$1/3-Ne(H)$** in the supersonic expansion. Second, ν_{OH} of **$1/3-Ne(H)$** can be estimated by comparing the complexation-induced shifts ($\Delta\nu_{OH}$ [$L_a \rightarrow L_b$]) for exchanging L_a with L_b in H-bound phenol^+-L and $o/p-C_6H_7O^+-L$ ($L_{a,b} =$ Ne, Ar, N_2). The OH group in phenol$^+$ is slightly more acidic than that in **1/3**, giving rise to slightly larger shifts. This small difference is demonstrated by the MP2 dissociation energies calculated for phenol^+-L ($D_e \approx 7.85$ and 22.85 kJ/mol for L = Ar and N_2) and **$3-L(H)$** ($D_e \approx 7.57$ and 21.63 kJ/mol for L = Ar and N_2), and by the larger $\Delta\nu_{OH}$ [Ar $\rightarrow N_2$] shift of phenol^+-L (-99 cm^{-1}) as compared to that of **$1/3-L(H)$** (-85 cm^{-1}). Both results indicate that the H-bonds in phenol^+-L are slightly stronger than those in **$1/3-L(H)$**. Thus, to estimate the (unknown) $\Delta\nu_{OH}$ [$L_a \rightarrow L_b$] shift of **$1/3-L(H)$**, a scaling factor of $85/99 \approx 0.86$ is applied to the (known) $\Delta\nu_{OH}$ [$L_a \rightarrow L_b$] shifts of phenol^+-L. Using this scaling factor and $\Delta\nu_{OH}$ [Ne $\rightarrow$ Ar] of phenol^+-L (-70 cm^{-1}),[30] $\Delta\nu_{OH}$ [Ne $\rightarrow$ Ar] of **$1/3-L(H)$** is estimated as -60 cm^{-1} and B_1 of **$1/3-Ne(H)$** is predicted at ≈3553 cm^{-1}, in good agreement with the experimental observation. In conclusion, the 3552 cm^{-1} peak in the $C_6H_7O^+-Ne$ spectrum is attributed to the overlapping B_1 and A_1 transitions arising from **$1/3-Ne(H)$** and **$5-Ne(H)$**, respectively. Although part of the signal at 3552 cm^{-1} may also originate from ν_{OH} of **$1/3-Ne(\pi)$** (B_1^π), the contribution of this isomer is probably minor.

In summary, major absorptions in the IRPD spectra of $C_6H_7O^+-L$ (L = Ne, Ar, N_2) are analyzed in terms of H-bound $C_6H_7O^+-L$ dimers composed of **1/3** and **5**. For **$1/3-Ar$**, also the π-bound structure is detected as a less stable isomer. The spectra of larger $C_6H_7O^+-L_n$ clusters (L = Ar and N_2, $n = 2-6$) discussed elsewhere[52] support the given assignments.

4. Further Discussion

The complexation-induced shifts, band profiles, and relative intensities in the IRPD spectra of $C_6H_7O^+-L$ unambiguously identify (at least) two different $C_6H_7O^+$ ions in the supersonic plasma expansion: the oxonium isomer ($O-C_6H_7O^+$, **5**) and the *ortho* and/or *para* protonated carbenium isomer ($o/p-C_6H_7O^+$, **1/3**). Complexes of $m-C_6H_7O^+$ (**2**) and $i-C_6H_7O^+$ (**4**) are not observed. Thus, in line with the theoretical predictions, the IR spectra demonstrate that **2** and **4** are substantially less stable than **1** and **3**. Although the calculations in Table 1 suggest that **5** is considerably lower in energy than previously predicted using smaller basis sets,[23,31] the relative energy difference between this isomer and the global minimum **3** is still substantial ($E_{rel} = 47$ and 77 kJ/mol at the MP2 and B3LYP levels). Thus, the experimental detection of **5** shows that there is no thermal equilibrium between the different $C_6H_7O^+$ isomers produced in the employed supersonic EI (cluster) ion source. The same conclusion is apparent from the IRPD spectra of $C_6H_7O^+-Ar$ in Figure 5. The detection of complexes of **5** in the EI source is rationalized by its large barrier for rearrangement toward **1–4**: once **5** is formed and cooled, efficient isomerization toward the more stable carbenium ions is hindered by $V(\mathbf{5} \rightarrow \mathbf{4}) = 162$ kJ/mol. Similarly, a large barrier separating

(50) Multiphoton absorptions can be excluded at the low laser intensities available (eq 6).[24,51]

(51) Solcà, N.; Dopfer, O. *Chem. Phys. Lett.* **2001**, *347*, 59.

(52) Solcà, N. Ph.D. Thesis, University of Basel, 2003.

Table 5. Experimental and Calculated Vibrational Frequencies of $O\text{-}C_6H_7O^+$ and $o/p\text{-}C_6H_7O^+$ (cm^{-1})[a]

isomer	vibration	experimental[a]	calculated[b]
$O\text{-}C_6H_7O^+$ (5)	$\nu_{OH,s}$	3502 ± 20	3480
	$\nu_{OH,as}$	3557 ± 20	3556
$o/p\text{-}C_6H_7O^+$ (1/3)	ν_{OH}	3558 ± 10	3564–3575
	ν_{CH} (sp^2)	$3046 \pm 10 / 3069 \pm 15$	3045–3069
	ν_{CH} (sp^3)	$2865 \pm 8 / 2877 \pm 8$	2843–2869

[a] The experimental values correspond to frequencies extrapolated from IRPD spectra of $C_6H_7O^+\text{-}L$ to zero solvation conditions (see text). [b] B3LYP/6-311G(2df,2pd) level. The values for $o/p\text{-}C_6H_7O^+$ correspond to the predicted frequency ranges of $cis\text{-}o\text{-}C_6H_7O^+$, $trans\text{-}o\text{-}C_6H_7O^+$, and $p\text{-}C_6H_7O^+$ (Table 1).

the fluoronium and carbenium ions of protonated fluorobenzene ($C_6H_6F^+$) was invoked to explain the detection of the less stable fluoronium isomer (besides the substantially more stable carbenium ions).[24,25] The efficient production of **5** (eq 4) is believed to be a consequence of kinetic rather than thermodynamic factors. In addition to $C_6H_7O^+$ generation, other factors determine the appearance of a particular $C_6H_7O^+\text{-}L$ cluster in the IRPD spectrum. These include the efficiency for $C_6H_7O^+\text{-}L$ cluster formation and the IR oscillator strength.[23] Because of the stronger intermolecular H-bonds of **5-L(H)** as compared to those of dimers of **1-4** and the correspondingly larger IR oscillator strengths (Tables 2 and 3, Figure 4), the IR detection of **5-L(H)** is favored over that of other $C_6H_7O^+\text{-}L$ dimers.[23,53]

The IR spectra of $C_6H_7O^+\text{-}L$ allow for an accurate extrapolation of the C−H and O−H stretch frequencies of the isolated $C_6H_7O^+$ isomers **1/3** and **5**. The results obtained are compared in Table 5 with the theoretical predictions. Aliphatic C−H stretch modes of **1/3** can directly be estimated from the dimer spectra as ν_{CH} (sp^3) = 2865 ± 8 and 2877 ± 8 cm^{-1}. For these modes, the ligands L act as a messenger with essentially no influence,[20,21] as demonstrated by the nearly L-independent ν_{CH} (sp^3) frequencies of **1/3-L** (B$_{2/3}$). The same is true for the aromatic ν_{CH} (sp^2) fundamentals, as was also observed in the IRPD spectra of $C_6H_7^+\text{-}L_n$.[20,21] In contrast to ν_{CH}, ν_{OH} values of H-bound $C_6H_7O^+\text{-}L$ are strongly L-dependent. Previous spectroscopic studies of related H-bound $XH^+\text{-}Rg$ dimers (Rg = He, Ne, Ar) revealed that for a given base X the complexation-induced frequency shifts, $\Delta\nu_{XH}$, scale roughly linearly with the proton affinity (PA) of the Rg ligand.[26,29] Extrapolation of $\Delta\nu_{XH} \to 0$ for a large variety of bases X resulted in an X-independent PA value, PA$_0$ = 166.7 ± 4.1 kJ/mol.[29] This result can be exploited here to estimate ν_{OH} of **1/3** as 3561.9 ± 5 cm^{-1}.[54] Alternatively, ν_{OH} of **1/3** may directly be estimated from ν_{OH} of **1/3-Ar(π)** (B$_1^\pi$ = 3554 cm^{-1}, fwhm =13 cm^{-1}), because for this isomer the Ar ligand has nearly no influence on the O−H bond.[30,47,48] The discrepancy of both extrapolations is on the order of the widths of the observed transitions, and ν_{OH} of **1/3** can safely be determined as 3558 ± 10 cm^{-1}. This value compares favorably with ν_{OH} predicted for **1** and **3** (3564–3575 cm^{-1}, Table 5).

The center frequency of $\nu_{OH,s}$ and $\nu_{OH,as}$ of $O\text{-}C_6H_7O^+$ ($\nu_{OH,av}$) is a measure for the O−H bond strength in **5** and may be extrapolated as 3530 ± 5 cm^{-1} by the procedure described above.[54] The splitting between $\nu_{OH,as}$ and $\nu_{OH,s}$ ($\Delta\nu_{OH,as-s}$) is related to the resonant coupling strength between the two local O−H oscillators and can be estimated in the following way.

First, the splitting between $\nu_{OH,b}$ and $\nu_{OH,f}$ in **5-L(H)** must be larger than $\Delta\nu_{OH,as-s}$ of **5**. This phenomenon is typical for H-bonding of L to one of two equivalent X−H donors and has been observed for a large number of related systems.[55−61] Second, $\Delta\nu_{OH,as-s}$ of the **5-Ar$_2$(H)** trimer is expected to be smaller than in bare **5**. This effect has been discussed, for example, for aniline$^+\text{-}L_n$ clusters (L = Ar and N$_2$)[55,56] and relies on the fact that the stretching force constants of the solvated X−H donor bonds are smaller than those of the (unsolvated) bonds (thus reducing the coupling strength). Using this information and the experimental O−H stretch frequencies of **5-Ne(H)** and **5-Ar$_2$(H)**,[23] $\nu_{OH,s}$ and $\nu_{OH,as}$ of **5** are estimated as 3502 ± 20 and 3557 ± 20 cm^{-1},[62] in good agreement with the predicted values of 3480 and 3556 cm^{-1} (Table 5).

Comparison of the derived $C_6H_7O^+$ frequencies with those of neutral phenol reveals the large influence of the protonation site on the properties of the OH group. In general, protonation significantly reduces the O−H bond strength, and the magnitude of this effect decreases in the order **5** > **1/3** > **2/4**. Quantitatively, ν_{OH} of phenol (3656 cm^{-1})[63] experiences a protonation-induced red shift of $\Delta\nu_{OH} = -126 \pm 5$ cm^{-1} for **5** (using $\nu_{OH,av}$), -98 ± 10 cm^{-1} for **1/3**, and ≈ -28 cm^{-1} for **2/4** (estimated from the calculations in the latter case). This trend is compatible with the calculated elongations of the O−H bond upon protonation: $\Delta R_{OH} \approx 0.012$ Å for **5**, ≈ 0.008 Å for **1/3**, and ≈ 0.003 Å for **2/4**. Consequently, the acidity of the O−H bonds in $C_6H_7O^+$ decreases along the series **5** > **1/3** > **2/4**, in line with the observed L-dependent frequency shifts for the bound O−H stretch modes of $C_6H_7O^+\text{-}L$. Figure 7 visualizes $\nu_{OH,av}$ of **5-L(H)** and ν_{OH} of **1/3-L(H)** as a function of PA$_L$. In line with PA$_{Ne}$ < PA$_{Ar}$ < PA$_{N_2}$, the intermolecular interaction increases along the series Ne < Ar < N$_2$, leading to decreasing O−H stretch frequencies. Because of its weaker and more acidic O−H bond, **5** is a better proton donor than **1/3**, in line with the larger dissociation energies of **5-L(H)** as compared to those of **1/3-L(H)** (Tables 2 and 3). Consequently, the decrease of $\nu_{OH,av}$ along the series Ne → Ar → N$_2$ in Figure 7 is more pronounced than that for ν_{OH}. As discussed in section 3.2, the acidity of the O−H bond in **1/3** is slightly smaller than that of phenol$^+$. Thus, the PA for O protonation of cyclic $o/p\text{-}C_6H_6O$ is concluded to be slightly larger than that of C_6H_5O (873 kJ/mol)[64] and can be estimated as 880 ± 10 kJ/mol.

It is illustrative to compare the carbenium ions of $C_6H_7O^+$ with the σ-complex of protonated benzene ($C_6H_7^+$) to elucidate the effect of H → OH substitution at different ring positions with respect to the CH$_2$ moiety. Ring-protonation of (substituted)

(53) For $O\text{-}C_6H_7O^+\text{-}N_2$, the observed cross section is probably complicated by the fact that $\nu_{IR} < D_0$ (see text).

(54) As described in ref 29, the linear relationship does not hold for H-bound N$_2$ complexes. Thus, for ν_{OH} extrapolated of $o/p\text{-}C_6H_7O^+$, the respective ν_{OH} values for L = Ne (3552 cm^{-1}) and L = Ar (3493 cm^{-1}) are used. In analogy, $\nu_{OH,av}$ of $O\text{-}C_6H_7O^+$ is extrapolated using $\nu_{OH,av}$ of the L = Ne (3514.5 cm^{-1}) and L = Ar (3431.5 cm^{-1}) complexes.

(55) Solcà, N.; Dopfer, O. *J. Phys. Chem. A* **2002**, *106*, 7261.

(56) Solcà, N.; Dopfer, O. *Eur. Phys. J. D* **2002**, *20*, 469.

(57) Roth, D.; Dopfer, O.; Maier, J. P. *Phys. Chem. Chem. Phys.* **2001**, *3*, 2400.

(58) Dopfer, O.; Roth, D.; Maier, J. P. *J. Chem. Phys.* **2001**, *114*, 7081.

(59) Roth, D.; Dopfer, O.; Maier, J. P. *Phys. Chem. Chem. Phys.* **2000**, *2*, 5013.

(60) Dopfer, O.; Nizkorodov, S. A.; Olkhov, R. V.; Maier, J. P.; Harada, K. *J. Phys. Chem. A* **1998**, *102*, 10017.

(61) Dopfer, O.; Roth, D.; Maier, J. P. *J. Chem. Phys.* **2000**, *113*, 120.

(62) Inversion tunneling of the OH$_2$ group, with barriers of 2.5 (B3LYP) and 5.7 (MP2) kJ/mol, possibly causes further shifts and splittings. No evidence for this splitting is observed in the dimer spectra.

(63) Bist, H. D.; Brand, J. C. D.; Williams, D. R. *J. Mol. Spectrosc.* **1967**, *24*, 402.

(64) Kim, H.; Green, R. J.; Qian, J.; Anderson, S. L. *J. Chem. Phys.* **2000**, *112*, 5717.
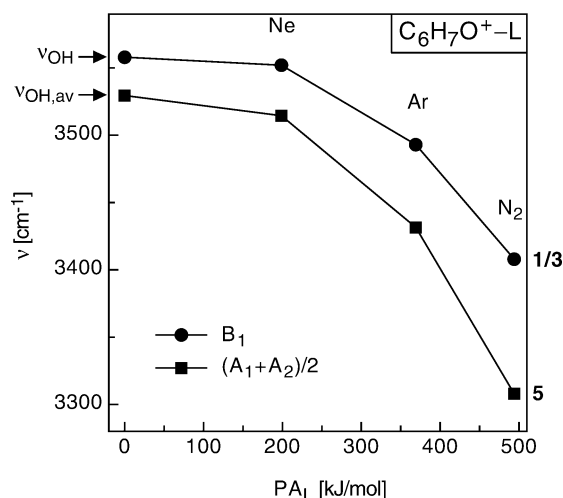
Figure 7. Plot of $\nu_{OH,av}$ of **5**−**L(H)**, (A$_1$ + A$_2$)/2, and ν_{OH} of **1/3**−**L(H)**, B$_1$, versus the proton affinity of the ligand, PA$_L$ (L = Ne, Ar, N$_2$).[45] The extrapolation to the free ν_{OH} and $\nu_{OH,av}$ frequencies of bare **1/3** and **5** is described in the text.

aromatic molecules induces a hybridization change of the protonated C atom from sp^3 to sp^3. The two aliphatic C−H stretch modes of C$_6$H$_7$$^+$ were observed at ν_{CH} (sp^3) $\approx$ 2795 and $\approx$2810 cm^{-1}.[20] The calculations predict ν_{CH} (sp^3) of **2** between 2803 and 2814 cm^{-1} (Table 1), indicating that the aliphatic C−H bonds of C$_6$H$_7$$^+$ and **2** are very similar. In contrast, ν_{CH} (sp^3) values of **1/3** are shifted to higher frequencies by $\approx$60−70 cm^{-1} (Table 5), implying that the aliphatic C−H bonds in **1/3** are considerably stronger and less acidic than those in C$_6$H$_7$$^+$ and **2**. The opposite trend seems to hold for the aromatic C−H bonds: ν_{CH} (sp^2) values of **1/3** at 3046 and 3069 cm^{-1} are lower than ν_{CH} (sp^2) of C$_6$H$_7$$^+$ (3081 and 3110 cm^{-1}), demonstrating that the OH group in **1/3** destabilizes these C−H bonds. The relative positions of ν_{OH} and ν_{CH} (sp^3) of **1/3** and **2** are in line with their AIM analysis:[65] transfer of electron density from the OH to the CH$_2$ group lowers the energy of **3**, and at the same time weakens the O−H bond and strengthens the aliphatic C−H bonds. This stabilizing effect is absent in **2**. Hence, the IR spectrum of **1/3** deduced in the present work provides direct spectroscopic confirmation of the strongly activating and *ortho*/*para* directing nature of the OH group in electrophilic aromatic substitution reactions.[65]

The intermolecular attraction in weakly bound cation$^+$−L dimers is dominated by electrostatic and inductive forces.[26,66] For **5**−**L** and **1/3**−**L**, these contributions stabilize H-bonds more than π-bonds, because the protons of the acidic OH groups in **1/3** and **5** carry a large positive partial charge (q_H = 0.67e for **1a/3** and 0.72e for **5**). Consequently, **5**−**L(H)** and **1/3**−**L(H)** are the preferred dimer structures (global minima) of **5**−**L** and **1/3**−**L**. Similar to the related phenol$^+$−L dimers,[30,48] the π-bound local minimum of **1/3**−**L** could be detected for L = Ar but not for L = N$_2$. The π-bound isomer of **5**−**L** could not be observed so far, and it is not even clear whether **5**−**L(π)** is a local minimum on the PES. The large L-dependent influence of H-bonding on the IR spectra of C$_6$H$_7$O$^+$−L requires the variation of L to extrapolate to the O−H bond properties of

isolated C$_6$H$_7$O$^+$. This is in contrast to the C−H stretch range, in which the IR spectra of C$_6$H$_7$O$^+$−L (L = Ne, Ar, and N$_2$) closely resemble that of bare C$_6$H$_7$O$^+$. The intermolecular interactions in C$_6$H$_7$$^+$−L are rather different from those in C$_6$H$_7$O$^+$−L. The H atoms in C$_6$H$_7$$^+$ carry only small partial charges of q_H = 0.12e (sp^2 hybridization of C) and 0.16e (sp^3 hybridization of C).[21] Thus, in the most stable C$_6$H$_7$$^+$−L structures, nonpolar ligands L prefer π-bonds to the ring (mainly stabilized by dispersion) over the weaker H-bonds to the CH donors.[20,21]

5. Concluding Remarks

Structural isomers of isolated protonated phenol (C$_6$H$_7$O$^+$) are characterized by IRPD spectroscopy and quantum chemical calculations of their weakly bound C$_6$H$_7$O$^+$−L dimers with L = Ne, Ar, and N$_2$. The complexes are generated in a supersonic plasma expansion coupled to electron ionization, which predominantly produces two major C$_6$H$_7$O$^+$ isomers: the oxonium ion **5** (*O*-C$_6$H$_7$O$^+$) and the carbenium ion(s) **1/3** (*o*/*p*-C$_6$H$_7$O$^+$). In contrast, the less stable isomers **2** (*m*-C$_6$H$_7$O$^+$) and **4** (*i*-C$_6$H$_7$O$^+$) are not observed. The most stable **1/3**−**L** and **5**−**L** dimers feature H-bonds between L and the OH donor groups, which is the preferred ion−ligand recognition pattern between these protonated phenol isomers and nonpolar hydrophobic solvent molecules. Extrapolation to zero solvation interaction (messenger approach) yields reliable experimental vibrational frequencies of bare *O*-C$_6$H$_7$O$^+$ and *o*/*p*-C$_6$H$_7$O$^+$. The symmetric and antisymmetric O−H stretch vibrations of *O*-C$_6$H$_7$O$^+$ are determined as $\nu_{OH,s}$ = 3502 $\pm$ 20 cm^{-1} and $\nu_{OH,as}$ = 3557 $\pm$ 20 cm^{-1}, and the O−H stretch mode of *o*/*p*-C$_6$H$_7$O$^+$ is derived as ν_{OH} = 3558 $\pm$ 10 cm^{-1}. Similarly, several C−H stretch modes of *o*/*p*-C$_6$H$_7$O$^+$ are deduced. In general, protonation of phenol induces chemically significant changes of the properties of its OH group. The O−H bonds become longer, weaker, and more acidic. The magnitude of these protonation-induced changes strongly depends on the protonation site and decreases along the series **5** > **1/3** > **2/4**. Comparison between the IR spectra of the carbenium ions of C$_6$H$_7$O$^+$ and the σ-complex of protonated benzene demonstrates the strongly activating and *ortho*/*para* directing nature of the OH group in isolated Wheland intermediates.

In conclusion, the fruitful combination of IR spectroscopy, mass spectrometry, and quantum chemistry is shown to provide a powerful tool to characterize fundamental properties of protonated aromatic molecules (AH$^+$) under controlled solvation conditions. Future efforts aim at the investigation of other AH$^+$ ions and related reactive intermediates using this successful strategy. Moreover, the present experimental approach can be utilized to probe in a stepwise fashion the sequential solvation of AH$^+$ in various solvent types. Eventually, such studies will bridge the gap between the different chemical properties of reactive intermediates in the gas and condensed phase.

(65) Bader, R. F. W.; Chang, C. *J. Phys. Chem.* **1989**, *93*, 5095.
(66) Dopfer, O. *J. Phys. Chem. A* **2000**, *104*, 11693.
(67) Sheng, Y.; Leszczynski, J. *Collect. Czech. Chem. Commun.* **2003**, *68*, 489.